Experimental Investigation of Bricks Under Uniaxial Tensile Testing

by

P B LOURENÇO[1], J C ALMEIDA[2], J A BARROS[1]
[1] University of Minho, Department of Civil Engineering, P-4800-058 Guimaraes, Portugal
[2] Instituto Piaget, ISEIT/VISEU, Estrada do Alto do Gaio, P-3510-651 Viseu, Portugal

ABSTRACT

Softening is a gradual decrease of mechanical resistance resulting from a continuous increase of deformation imposed on a material specimen or structure. It is a salient feature of quasi-brittle materials like clay brick, mortar, ceramics, stone or concrete which fail due to a process of progressive internal crack growth. Such mechanical behaviour is commonly attributed to the heterogeneity of the material, due to the presence of different phases and material defects, such as flaws and voids. For tensile failure this phenomenon has been well identified for concrete but very few results exists for clay brick. In the present paper, the results of an extensive set of tests carried out at University of Minho and including three different types of brick under uniaxial tension will be presented. Both tensile strength and fracture energy are quantified, with recommendations for the adoption of practical values.

1. INTRODUCTION

The tensile behaviour of concrete and other quasi-brittle materials that have a disordered internal structure, such as brick, can be well described by the cohesive crack model proposed initially by HILLERBORG [1]. This model has been widely used as the fundamental model that describes the non-linear fracture mechanics of quasi-brittle materials, e.g. [2,3]. According to this model and due to cracking localization, which is a characteristic of fracture process in quasi-brittle materials, the tensile behaviour is characterized by two constitutive laws associated with different zones of the material during the loading process, see Figure 1. The elastic-plastic stress-strain relationship of Figure 1a is valid until the peak load is reached. It is noted that before the peak inelastic behaviour occurs due to micro-cracking and the energy dissipated in this process is usually neglected for the calculation of the fracture energy. The stress-crack opening displacement relationship of Figure 1b describes the strain softening behaviour in the fracture process zone after the peak. The cohesive stress-opening displacement diagram is characterized by the gradual decrease of stress from its maximum value to zero, corresponding to the increase of the distance between the two edges of the crack from zero to the critical opening, u_c. The softening diagram assumes a fundamental role in the description of the fracture process and is characterized by the tensile strength, f_t, and the fracture energy, G_f, which is given by the area under the softening diagram, see Figure 1b. The critical crack opening, u_c, can be replaced by the ductility index d_u [4] given as the ratio G_f / f_t, which represents the fracture energy normalized by the tensile strength. This parameter allows the characterization of the brittleness of the material and is directly related to the shape of the descending portion of the stress-deformation diagram.

There are several experimental methods that have been used to measure the fracture properties (tensile strength, fracture energy and ductility index) that allow the definition of the constitutive laws of the material, namely direct tensile tests, indirect tensile tests such as the three-point load test, and the Brazilian splitting test. Although tensile failure results from a load combination and a multiplicity of factors, meaning that direct tension is not the only cause of tensile cracking, a direct tensile test seems to be the most appropriate test to characterize the basic failure mechanism (mode I) of quasi-brittle materials. This test is defined as the reference method to follow [5] being adopted in this work for the characterization of the tensile behaviour of bricks.

Different issues related to the specimens and the test procedures have been discussed in the past, namely the testing equipment, the control method, the location of the Linear Variable Displacement Transducers (LVDTs), the alignment of the specimen and, especially, the attachment of the specimens to the steel platens. The relevance of the latter is addressed in Figure 2 [5]. The behaviour in Figure 2a (rotating platens or hinges) is justified by the rotation of the specimen during the loading operation, where the crack proceeds from one side of the specimen to the other side. In the case of Figure 2b using fixed (non-rotating) platens, a bending moment is introduced and multiple cracks will appear. This results in a slightly larger tensile strength and a higher value of energy dissipated (fracture energy). Finally, it is noted that although the tensile strength and fracture energy are considered intrinsic properties of the material, it is well known that fracture properties are size and scale dependent [6,7].

Tensile fracture parameters of masonry constituents, namely units and the mortar-unit interface, are key parameters for advanced numerical modelling of masonry and for a deeper understanding of the behaviour of masonry structures. In the present paper, an experimental programme using three types of clay brick is discussed with the objective of increasing the data available in the literature.

2. TEST SET-UP AND SPECIMENS

Tensile tests were performed with solid bricks produced by Vale da Gândara, Portugal(S), hollow bricks produced by J. Monteiro e Filhos, Portugal (HP), and hollow bricks produced by Suceram, Spain (HS). All bricks are extruded and they were tested in vertical or thickness (V) and in horizontal or length (H) direction resulting in six series with the following notation: SV, SH; HPV, HPH; HSV, HSH. Table 1 gives the dimensions of the bricks and the free water absorption. The net compressive strength of the bricks, along the extrusion direction was 78N/mm^2, 82N/mm^2 and 58N/mm^2, respectively for S, HP and HS. Here it is noted that these values are merely indicative, as the first two values were from independent tests by different researchers and insufficient information about the testing procedures is available, see [8,9]. The third value of compressive strength was provided by the manufacturer.

It is noted that: (a) bricks HP are extruded with the holes parallel to the larger dimension and bricks HS are extruded with the holes parallel to the smaller dimension; (b) bricks HP and HS have small grooves in the upper surface (side opposite to the facing side) in order to increase adhesion between the unit and the backing mortar, see Figure 3.

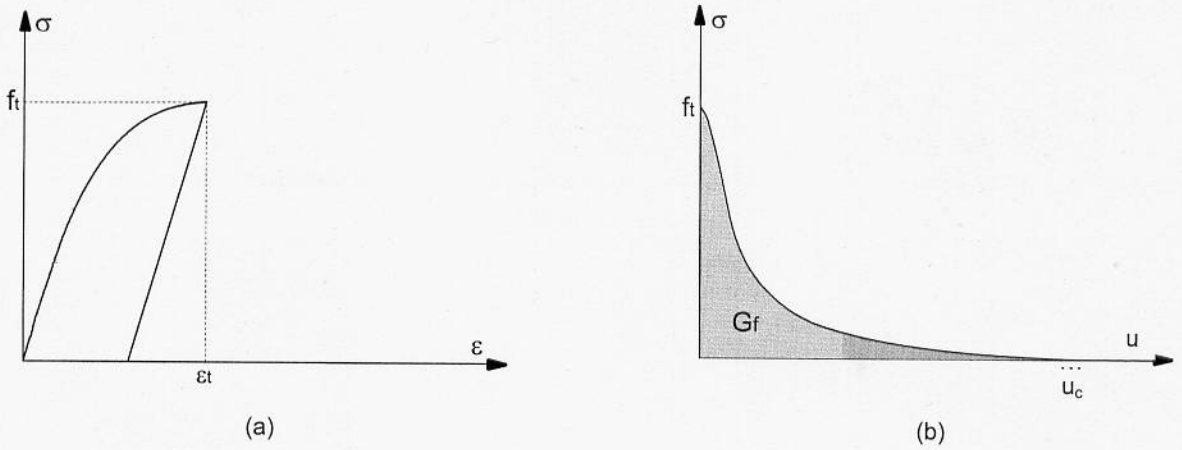

Figure 1 General cohesive model: (a) elastic stress-strain diagram; (b) stress-crack opening displacement diagram

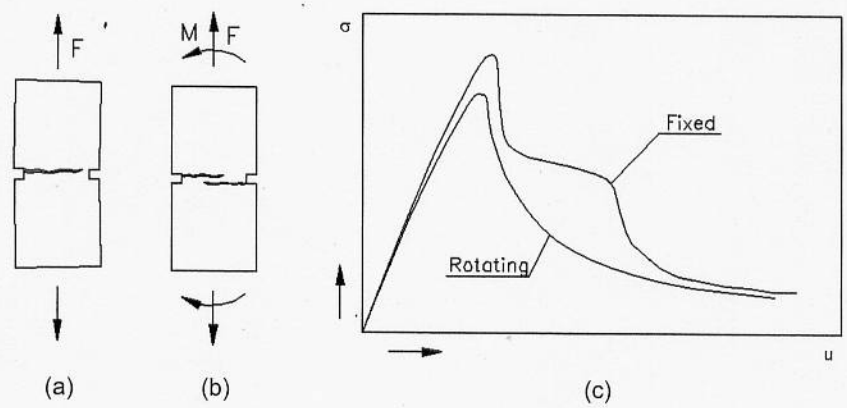

Figure 2 Influence of boundary conditions: (a) pin-ended boundary; (b) clamped boundary; (c) effect on the softening shape

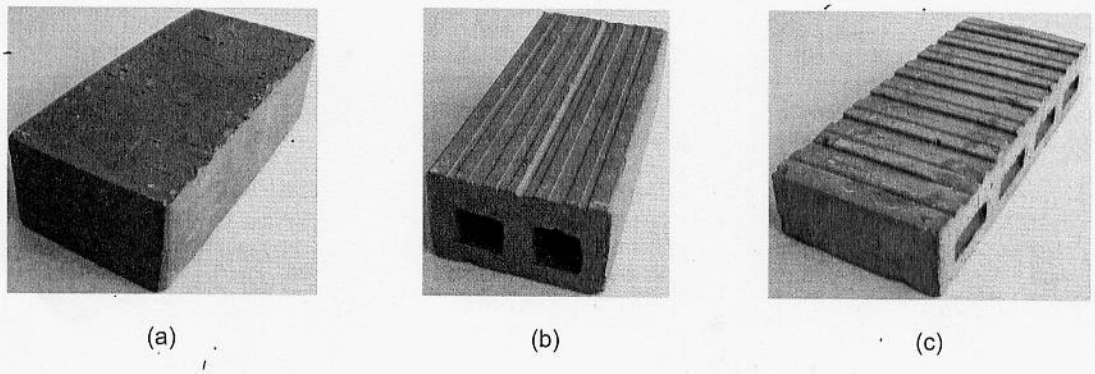

Figure 3 Selected bricks for testing: (a) S brick; (b) HP brick; (c) HS brick

Table 1
Series of brick specimens: dimensions and absorption

Bricks	Dimensions [mm]	Free water absorption [mass-%]
S	220 × 110 × 70	9.7
HP	220 × 110 × 70	10.6
HS	240 × 100 × 50	14.6

2.1 Testing equipment and applied measuring devices

The tests were performed in the laboratory of the Civil Engineering Department of University of Minho, using a CS 7400 – S shearing testing machine. This machine has two independent hydraulic actuators, positioned in vertical and horizontal directions. It has a load cell connected to the vertical actuator with a maximum capacity of 25 kN, being particularly suited to small specimens (maximum size of 90 x 150 x 150mm).

The adoption of a constant cross section for the specimens leads to uncertainty about the location of the micro-cracks. This represents the usual supplementary difficulty for the control method of this type of test. Since the control system allows only one Linear Variable Displacement Transducer (LVDT) as displacement control, it was decided to introduce, by means a diamond sawing machine, two lateral notches with a depth of 8mm and a thickness of 3mm at mid height of the specimen in order to localize the fracture surface. With the notches, the stress and deformation distribution is no longer uniform, with stress and strain gradients occurring very localized near the notch tips.

Since three-dimensional non-uniform crack opening can occur on tensile tests [10], the tensile test control using the average of the deformations registered on the four corners of the specimen is the most appropriate procedure, see Figure 4. However, the available equipment can only control one displacement transducer (LVDT), located at a notched side. The transducers have a measure base of 1mm with a linearity of 0.17% of the full stroke. A deformation rate of 0.5μm/s was used in the tests. The force applied was measured on a load cell of 25kN maximum load bearing capacity, with an accuracy of 0.03%.

After preparation of the specimens' ends, glue adhesion conditions were enhanced by making a series of superficial slots with a saw. Then, the specimens were carefully fixed to the steel platens using an epoxy resin (DEVCOM) in such a way that the platens were kept perfectly parallel. Here, it is noted that the steel platens are fixed (non-rotating), meaning that load eccentricity is not an issue for prismatic specimens. The only source of eccentricity is the lack of parallelism between the steel platens which would induce a bending moment in the specimen in the clamping operation.

2.2 Specimen dimensions

Taking into consideration the brick dimensions and the test set-up, 40 x 40 x 70mm S brick specimens were extracted as shown in Figure 5. HP and HS bricks are hollow and, therefore, the specimens extracted from the bricks must be representative of the brick shell, a channel or U specimens, and the brick web I specimens, see Figure 6. Here, it is noted that the usage of channel specimens in questionable because a load eccentricity is introduced by the fact the top and bottom flanges are fully glued to the steel specimens. Nevertheless, because the end platens are fully fixed, the eccentricity is very low: a linear elastic FEM calculation indicates that the normalized load eccentricity (measured by eccentricity / web width) is only 0.03.

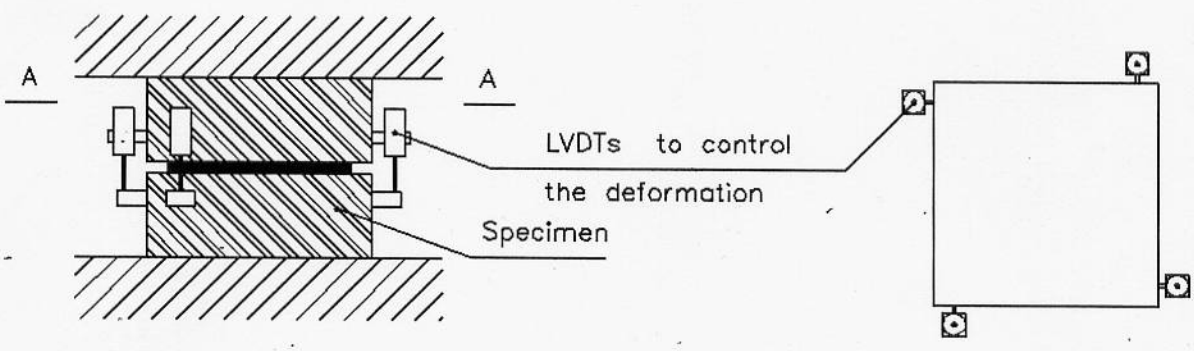

(a)

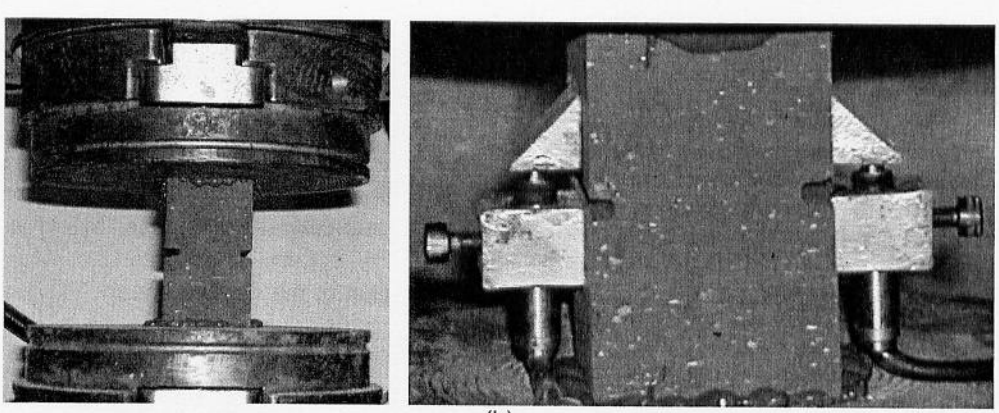

(b)

Figure 4 Test set-up: (a) preferred location of LVDTs for direct tensile tests; (b) front view including platens and details of LVDT placement

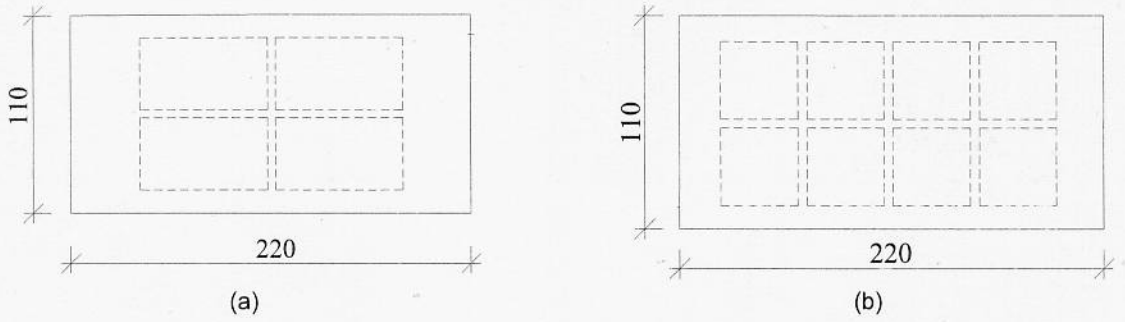

Figure 5 Solid bricks: (a) SH specimens; SV specimens

Figure 6 Typical specimens for hollow bricks: (a) shell, channel or U specimen; (b) web or I specimen

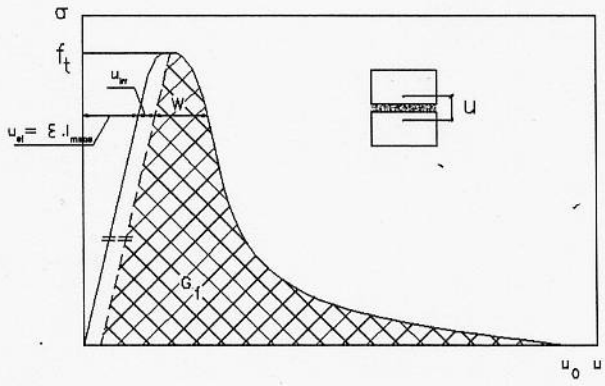

Figure 7 Schematic representation of the procedure to evaluate the fracture energy, G_f

3. RESULTS

From the force-elongation relationship obtained in the tensile tests, the following parameters were evaluated: tensile strength, fracture energy, and residual stress at ultimate scan reading. The notches reduce the Young's modulus of the brick (E_b) by about 20% – 40% [11]. As the measure of E_b is questionable, it is not shown here.

Figure 7 illustrates the procedure adopted for evaluating the fracture energy, G_f. In the cohesive crack model addressed above, the crack opening u is equal to the total elongation, subtracted from the elastic deformation ($u_{el} = \sigma$ x l_{meas} / E_0) and the irreversible deformation u_{irr}, which accounts for inelastic effects during material unloading, in the vicinity of the macro-crack. Here, l_{meas} is the distance between the measuring points of the LVDT.

The maximum force recorded by the load cell was divided by the effective area of each specimen (notched cross-section), in order to determine the tensile strength.

The fracture energy is identified with the work that is carried out to complete the separation of the two faces of the macro-crack, per unit of area. It is not possible to determine the exact crack opening for which the stress value transferred becomes zero, due to long tail exhibited by the softening branch of the stress-opening crack. For the calculation of the fracture energy, the value of the fracture energy is usually calculated as the result of the sum of two quantities, one quantity being measured and the other quantity estimated. The measured value of fracture energy $G_{f,meas}$ is directly computed as the area under the stress-crack opening diagram up to a nominal value of the peak strength (or the ultimate value). The estimated value $G_{f,est}$ is calculated as the area under the linear curve obtained by linear [12] or non-linear [11] adjustment of the original diagram below the cut-off.

Here, taking into account the force-elongation diagrams and the internal friction of the testing equipment, the fracture energy was simply evaluated up to a deflection of 60μm or up to a deflection corresponding to a force of 200N (if the deflection is less than 60μm). For the tests aborted before these limit conditions, the energy dissipated was not evaluated.

3.1 S specimens

The stress-elongation relationships for specimens SV and SH are depicted on Figure 8. For specimens SV (in the extrusion direction), the average values were 3.48N/mm^2 (42%) for the tensile strength and 0.0575N/mm (39%) for the fracture energy. The ductility index, again given by the ratio G_f / f_t, was 0.0165mm. The values inside brackets indicate the values of the coefficients of variation (CV) for the sixteen successful tests. For specimens SH (perpendicular to the extrusion direction), the average values were 2.96N/mm^2 (63%) for the tensile strength and 0.0508N/mm (41%) for the fracture energy. The values inside brackets indicate the values of the coefficients of variation for the fourteen successful tests. The ductility index was 0.0172mm.

The tensile strength in the extrusion direction was 4.5% of the compressive strength. The tensile strength in the extrusion direction was18% higher and the fracture energy is 15% higher than the values obtained in the perpendicular direction, due to the alignment of the microstructure. The ductility was similar in both directions. Therefore, brick type S exhibited only moderate anisotropy.

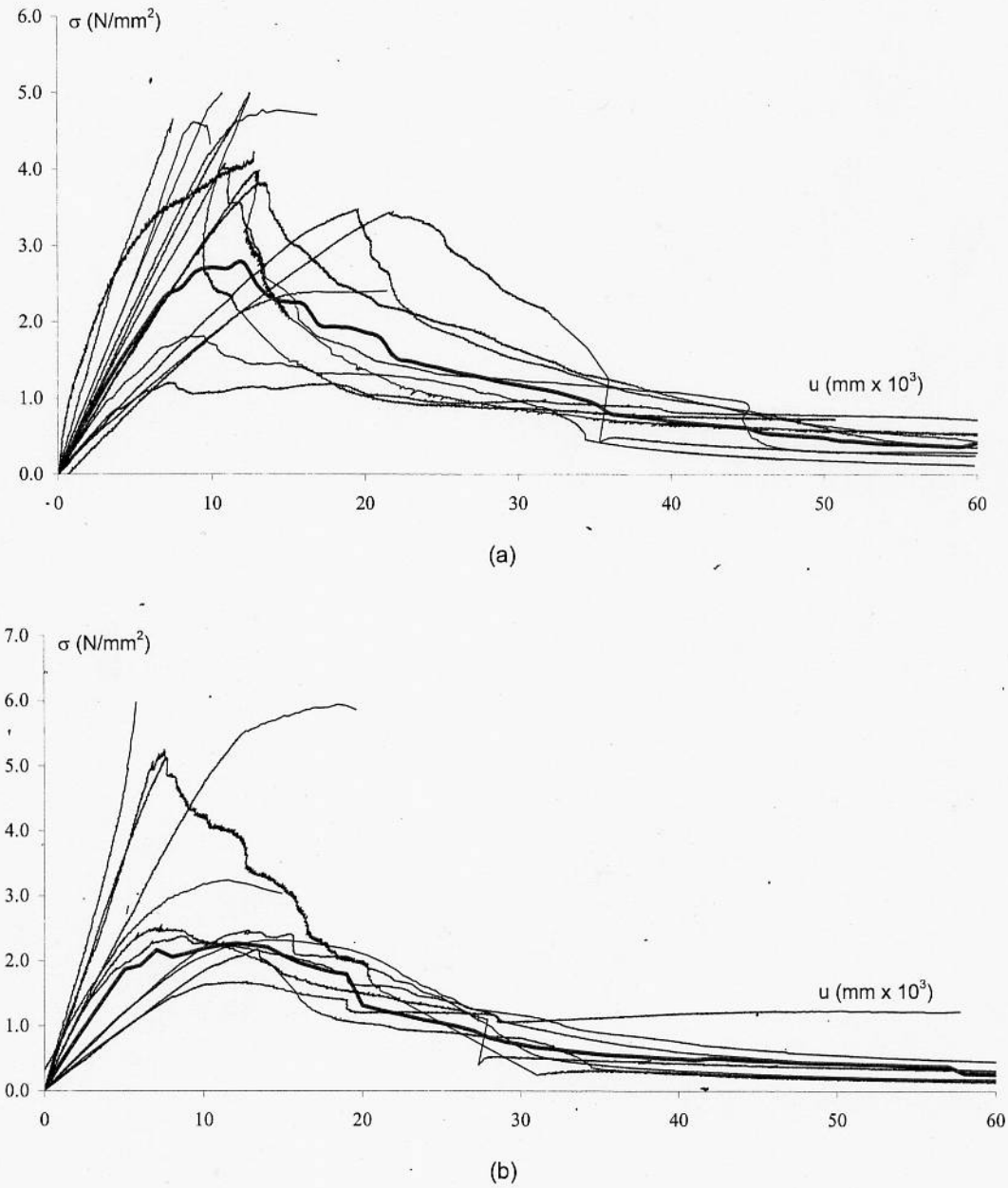

Figure 8 Stress-elongation for S brick specimens: (a) SV; (b) SH. The thicker line is the average of all specimens

All the results exhibit very a large scatter, though the scatter was higher in the direction perpendicular to the extrusion direction. The reason for this seems to be flaws, micro-cracks and inclusions in the burnt clay. It is well known that the fracture process is a three-dimensional process [10] and Figure 9a illustrates the typical superficial cracking patterns of brick specimens. It is clear that both straight and pronounced S-shaped cracks appear, meaning that a large scatter must be found. In all cases, the cracking surface was tortuous, going around the aggregate and concentrating in the interfaces between the aggregate and the matrix.

Finally, the results of the fracture energy vs. the tensile strength were plotted in Figure 10, where it can be seen that there was a weak correlation between fracture energy and tensile strength, although a clear trend for fracture energy to increase with an increase of tensile strength was found.

3.2 HP specimens

The stress-elongation relationships for specimens HPV and HPH are depicted on Figure 11. For specimens HPV (perpendicular to the extrusion direction), the average values were 2.86N/mm^2 (49%) for the tensile strength and 0.0557N/mm (41%) for the fracture energy. The ductility index was 0.0195mm. The values inside brackets indicate the values of the coefficients of variation for the twenty-three successful tests. For specimens HPH (in the extrusion direction), the average values were 4.32N/mm^2 (57%) for the tensile strength and 0.0853N/mm (52%) for the fracture energy. The values inside brackets indicate the values of the coefficients of variation for the fourteen successful tests. The ductility index was 0.0197mm.

The tensile strength in the extrusion direction was 5.3% of the compressive strength. The tensile strength in the extrusion direction was 53% higher and the fracture energy is 53% higher than the values obtained in the perpendicular direction. The ductility was similar in both directions but brick type HP exhibited considerable anisotropy.

Again, all the results exhibited very large scatter although the scatter was higher in the direction parallel to the extrusion direction. As mentioned above, this series consisted of specimens with U (channel) and I cross-section. The results in terms of fracture parameters f_t, G_f and d_u, sorted by specimen type, are now given in Table 2. It is clear from the results that the brick shell (U specimen) had a tensile strength much higher than the brick web (I specimen), whereas the fracture energy of the shell was similar to the fracture energy of the web. This seems to be related to micro-cracking of the unit, which controls mainly the tensile strength and was higher in the external part due to drying shrinkage, while the composition of the brick clay was the same in both cases and controls mainly the fracture energy.

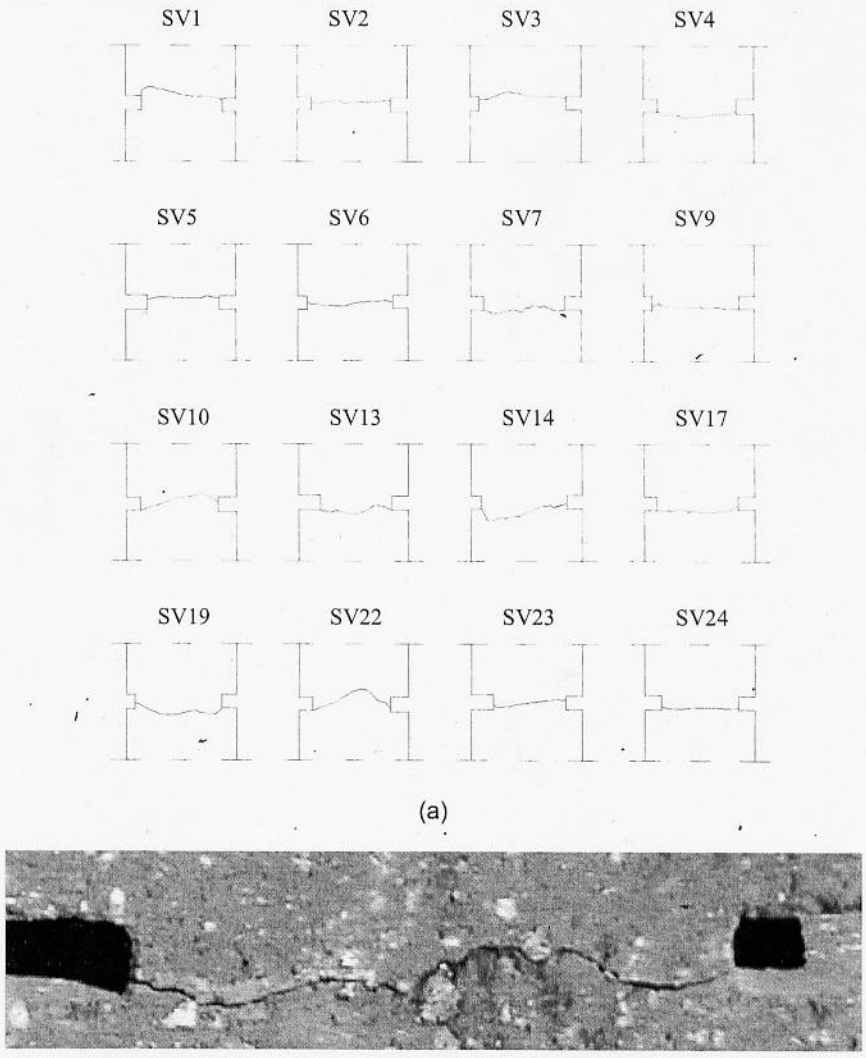

Figure 9 Examples of the cracking pattern for specimens SV: (a) all specimens; (b) detail

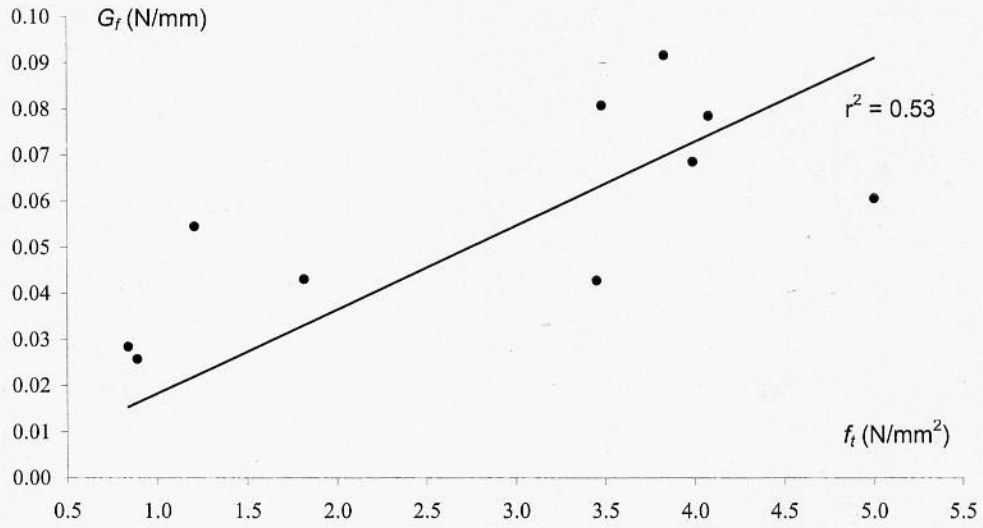

Figure 10 Correlation between fracture energy and tensile strength (specimens SV)

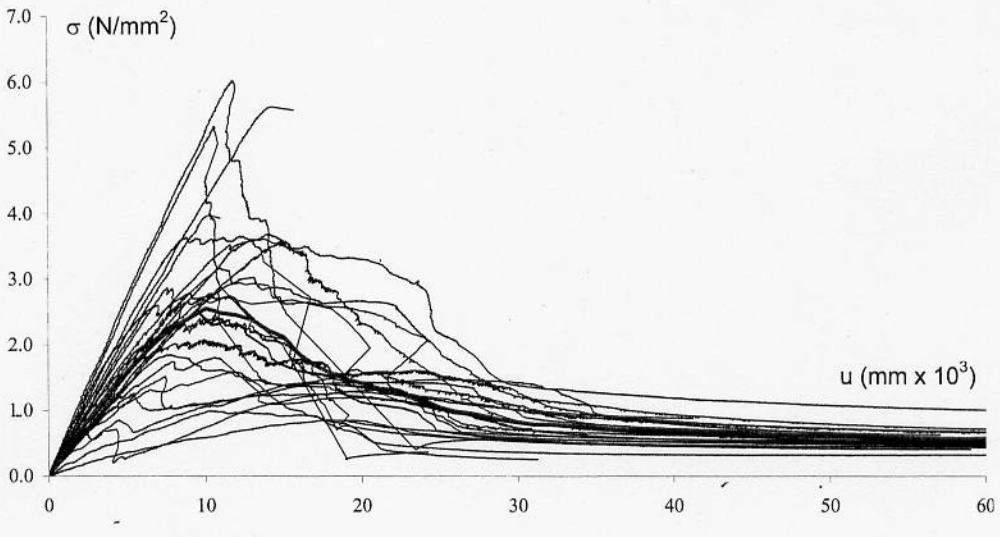

(a)

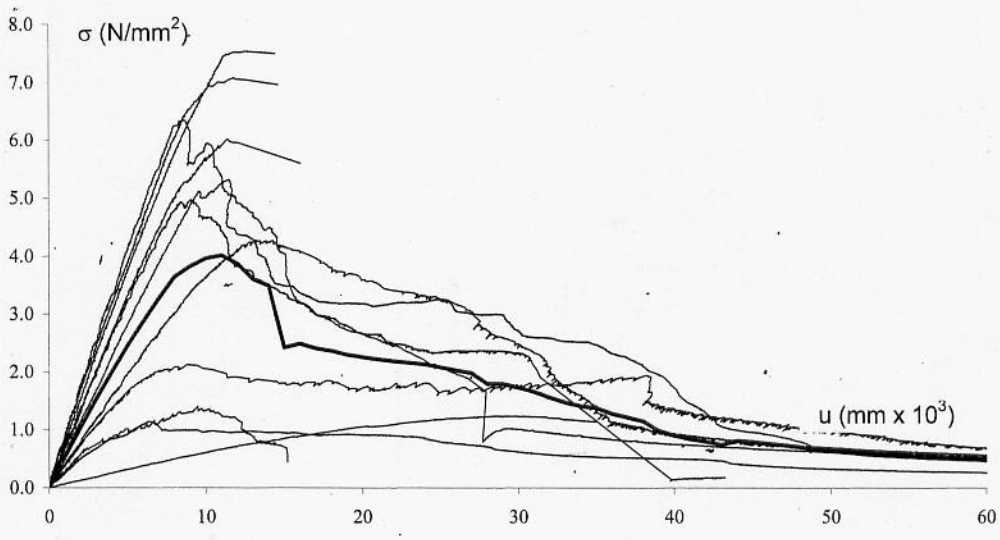

(b)

**Figure 11 Stress-elongation for HP brick specimens:
(a) HPV; (b) HPH. The thicker line is the average of all specimens**

Finally, it is noted that the very large number of specimens considered for HPV series resulted from the early observation that the peak values had enormous variations (tensile strength between 0.86 and 6.03N/mm^2), although a few specimens failed in an uncontrolled way due to the location of the fracture surface outside the notches, see Figure 12a. In the case of HPH series, there was a significant number of unsuccessful specimens due to the combination of high strength and low bond area, see Figure 12b. The plant where the bricks were produced has not been modernized and the firing temperature is not uniform, which can also partly explain the scatter found.

3.3 HS specimens

The stress-elongation relationships for specimens HSV and HSH are depicted in Figure 13. For specimens HSV (perpendicular to the extrusion direction), the average values were 2.75N/mm^2 (27%) for the tensile strength and 0.0573N/mm (32%) for the fracture energy. The ductility index was 0.0208mm. The values inside brackets indicate the values of the coefficients, of variation for the nine successful tests. For specimens HSH (in the extrusion direction), the average values were 3.82N/mm^2 (32%) for the tensile strength and 0.0572N/mm (40%) for the fracture energy. The values inside brackets indicate the values of the coefficients of variation for the thirteen successful tests. The ductility index was 0.0150mm.

The tensile strength in the extrusion direction was 6.6% of the compressive strength. The tensile strength in the extrusion direction was 39% higher than the values obtained in the perpendicular direction and the fracture energy was the same in both cases. Therefore, the ductility was different in both directions and bricks type HS also exhibited a large anisotropy. Again, all the results exhibited a large scatter.

3.4Comparison between the different brick results

Table 3 presents condensed results that are of relevance for practical purposes. Here, f_t is the tensile strength, f_c is the compressive strength, the subscripts // and $\perp$ indicate parallel and perpendicular to the extrusion direction respectively, and $d_{u,\,aver}$ is the average ductility index G_f / f_t including the directions parallel and perpendicular to extrusion. Taking into consideration that three different types of bricks have been considered, the difference in the results is moderate, with the exception of the anisotropy which exhibits significant differences between the types of brick.

The results indicate that: (a) the tensile strength in the extrusion direction was around 4.5-6.6% of the compressive strength (average value of 5%), reaching a value around 3.5-4.3N/mm^2 (average value of 3.9N/mm^2); (b) bricks exhibited moderate to high anisotropy for the tensile strength with $f_{t//} / f_{t\perp}$ around 1.2-1.5 (average value of 1.4); (c) the ductility index was around 0.017-0.020mm (average value of 0.018, i.e. an average fracture energy value of 0.07N/mm).

Table 2
Results for HP series, sorted by type of specimen (CV in brackets)

Specimen	f_t [N/mm^2]	G_f [N/mm]	d_u [mm]
HPV – U	3.38 (44%)	0.0576 (45%)	0.0170
HPV – I	1.99 (33%)	0.0529 (31%)	0.0266
HPH – U	5.62 (39%)	0.0865 (75%)	0.0154
HPH – I	2.75 (64%)	0.0843 (40%)	0.0307

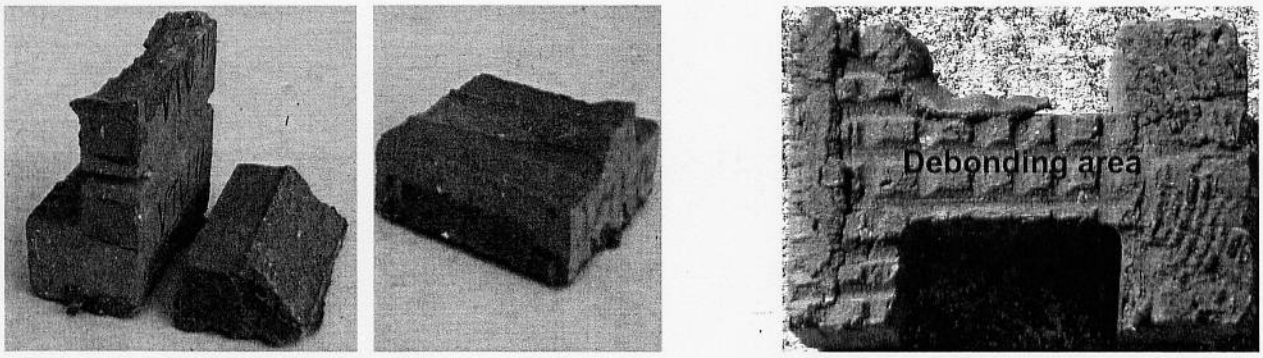

(a) (b)

Figure 12 Unsuccessful tests for HP brick specimens:
(a) failure surface outside the notched cross-section in HPV series; (b) difficulty in gluing HPH series

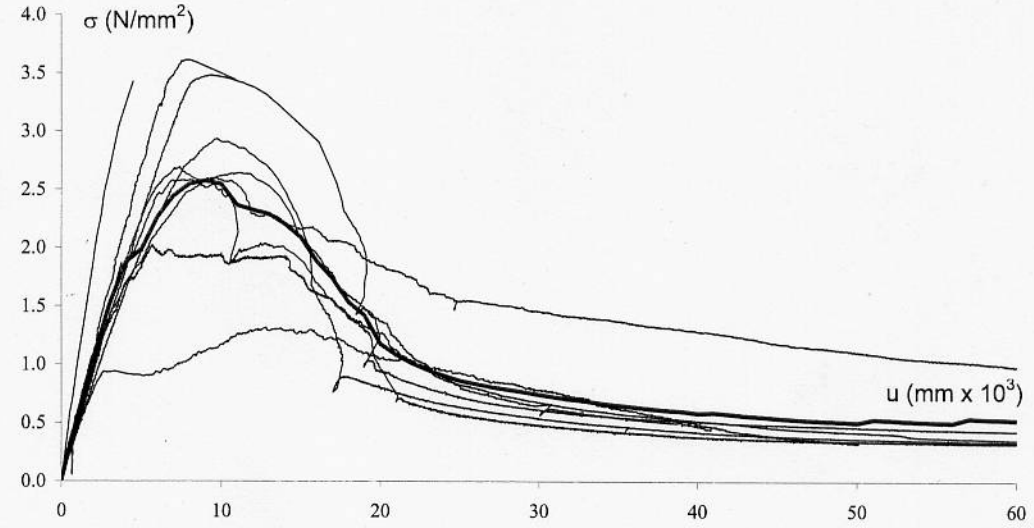

(a)

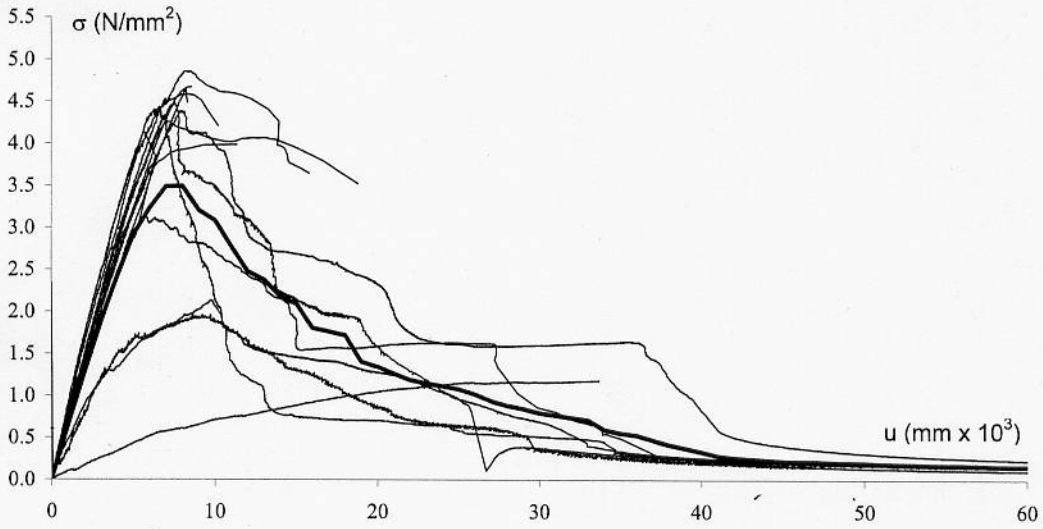

(b)

Figure 13 Stress-elongation for HS brick specimens: (a) HSV; (b) HSH. The thicker line is the average of all specimens

Table 3
Average results for all brick series

Bricks	$f_{tl/}$ / $f_{cl/}$ [-]	$f_{tl/}$ / $f_{t\perp}$ [-]	$f_{tl/}$ [N/mm²]	$d_{u,\ aver}$ [mm]
S	4.5%	1.18	3.48	0.0169
HP	5.3%	1.53	4.32	0.0196
HS	6.6%	1.39	3.82	0.0179
Average	5%	1.4	3.9	0.018

4. CONCLUSIONS

The present paper aims to discuss the tensile behaviour of bricks and provide data for advanced numerical simulations. For this purpose, three different producers were selected including solid and hollow bricks from Portugal and Spain. Direct tensile tests on a servo-controlled machine were carried out in order to obtain the tensile strength, the fracture energy and the shape of the stress-elongation diagram.

All bricks were tested in two orthogonal directions, namely along and normal to the direction of extrusion. For the hollow bricks, two different types of specimen were extracted so that the shell and the web could be characterized. Due to the presence of voids and internal firing cracks, the complete stress-elongation diagram could not be obtained in several of the specimens.

The results indicate a large scatter for the tensile strength and fracture energy. The following conclusions with respect to the tensile strength are possible: (a) bricks possess anisotropy with higher strength in the direction parallel to extrusion; (b) in hollow bricks, the tensile strength of the shell is higher than that of the web. Moreover, the average results in the brick specimens are fairly constant taking into consideration that three different brick manufacturers were involved. Therefore, for practical purposes the following recommendations seem possible: (a) the tensile strength of brick is around 5% of the compressive strength (with values found around $4N/mm^2$ in the direction parallel to extrusion and $3N/mm^2$ in the direction perpendicular to extrusion); (b) the ductility index is around 0.018mm (meaning that the fracture energy found is around 0.08 and 0.06N/mm, respectively parallel and perpendicular to the extrusion direction). The values found apply solely for solid bricks and must be reduced for hollow bricks, according to the volume of holes.

ACKNOWLEDGMENTS

The present work was partially supported by project GROW-1999-70420 "Industrialised solutions for construction of reinforced brick masonry shell roofs" funded by European Commission.

REFERENCES

1. HILLERBORG, A, MODEER, M, and PETERSSON, P E. Analysis of crack formation and crack growth in concrete by means of fracture mechanics and finite elements. Cement Concrete Research, **6**, 773-782, 1976.
2. BAZANT, P Z. Concrete fracture models: testing and practice. Engineering Fracture Mechanics, **69**, 165-205, 2002.
3. ELICES, M, GUINEA, G V, GÓMEZ, J, and PLANAS, J. The cohesive model: advantages, limitations and challenges. Engineering Fracture Mechanics, **69**, 137-163, 2002.
4. CHIAIA B, VAN MIER, J G M, and VERVUURT, A. Crack growth mechanisms in four different concretes: microscopic observations and fractal analysis. Cement Concrete Research, **28**, 103-114, 1998.
5. VAN MIER, J G M, and VAN VLIET, M R A. Uniaxial tension test for the determination of fracture parameters of concrete: State of the art. Engineering Fracture Mechanics, **69**, 235-247, 2002.
6. CARPINTERI, A, and FERRO, G. Size effects on tensile fracture properties: a unified explanation based on disorder and fractality of concrete microstructure, Materials and Structures, **27**, 563-571, 1994.
7. VAN VLIET, M R A, and VAN MIER, J G M. Experimental investigation of size effects in concrete and sandstone under uniaxial tension, Engineering Fracture Mechanics, **65**, 165-88, 2000.
8. OLIVEIRA, J T, LOURENÇO, P B, and BARROS, J O. Shear testing of stacked bonded masonry, Report 02-DEC/E-10, University of Minho, Portugal, 2002. Available from www.civil.uminho.pt/masonry.
9. SARRALBO, V. Contribution to the viability of laminar reinforced masonry roofs using semi-prefabricated solutions. Proposal for short span cylindrical shells (in Spanish), PhD Thesis, Universitat Politècnica de Catalunya, Barcelona, 2002.
10. HORDIJK, D A. Local approach to fatigue of concrete. PhD Thesis. Delft University of Technology, the Netherlands, 1991.
11. VAN DER PLUIJM, R. Out-of-plane bending of masonry behavior and strength, PhD Thesis. Eindhoven University of Technology, 1999.
12. VAN VLIET, M R A. Size effect in tensile fracture of concrete and rock. PhD thesis. Delft University of Technology, 2000.